Porous Materials

Direct Access to Bicontinuous Skeletal Inorganic Plumber's Nightmare Networks from Block Copolymers[**]

Anurag Jain, Gilman E. S. Toombes, Lisa M. Hall, Surbhi Mahajan, Carlos B. W. Garcia, Wolfgang Probst, Sol M. Gruner, and Ulrich Wiesner*

The co-assembly of organic and inorganic materials into a wide variety of structures at the nanoscale represents one of the most promising and exciting avenues for development of novel multifunctional materials.[1] A research area that has captivated researchers for some time is the synthesis and characterization of co-continuous nanostructures. Pioneering work in the field was done at Mobil Corp.[2,3] where a surfactant template was used to obtain mesoporous silica-type materials with enormous surface areas and pores larger than those accessible with conventional zeolites. The approach has since then been advanced to much larger pore sizes by utilizing block copolymers as templates.[4–7] The continuous nature of nanoscale channels combined with the unique structural and physical properties of these materials has sparked enormous interest for applications in areas such as catalysis, molecular separation, photonics, energy generation and storage, or electronics. Whereas most of the work in the field has been based on the so-called regular co-continuous structures in which the silica resides in the matrix of the bicontinuous mesophase,[8–13] relatively few examples exist of the more challenging reverse mesophases[14–17] in which the inorganic component forms the network channels. Moreover, all of these studies focused on cubic structures with $Ia\bar{3}d$ symmetry. Herein we report for the first time, to our knowledge, a simple approach to silica-based skeletal bicontinuous networks with $Im\bar{3}m$ symmetry in thick samples. Furthermore, the approach provides direct access to the skeletal networks thereby rendering time consuming backfilling procedures unnecessary. The as-made nanocomposite derived from a block-copolymer-directed sol–gel synthesis consists of silica networks embedded in an organic matrix. The structure is robust enough to undergo calcination at high temperatures, which gives the final skeletal silica networks (also known as nano-relief structures). Small angle X-ray scattering (SAXS) and transmission electron microscopy (TEM) data are consistent with the plumber's nightmare morphology (point group $Im\bar{3}m$) based on the P minimal surface (see Figure 4).[13,18,19] Proven modifications of the sol–gel process, to include transition-metal oxides,[20] or extension of the approach to non-oxide ceramics, such as SiCN and SiC,[21] may provide a unique approach to the straightforward design and fabrication of multifunctional skeletal networks in the future.

Many bicontinuous mesophases are based on minimal surfaces.[22] Minimal surfaces, which have zero mean curvature all across the surface, result from the requirement of area-minimization of the intermaterial dividing surface of two dissimilar materials. A large variety of intertwined 3D continuous structures based on these minimal surfaces have been computed mathematically and, for several systems, realized experimentally.[23,24] Extensive theoretical and experimental research has shown, however, that in classical block copolymers, energetic combined with space-filling requirements put considerable constraints on the equilibrium mesophases that can be obtained.[25] Indeed, the double gyroid mesophase has been the only bicontinuous phase that has been found to be stable in diblock copolymer systems in a highly restricted parameter space.[26] Similarly, most bicontinuous mesoporous inorganic materials obtained from organic templates also belong to the gyroid family.[8–11] By careful manipulation of the polymer–ceramic interface utilizing organically modified silica precursors (ormocers) and working from organic solvents, we have recently shown the existence of a new bicontinuous cubic phase in bulk organic–inorganic hybrids and mesoporous materials derived from it that is consistent with the plumber's nightmare morphology.[13,27] This result has opened the possibility for finding a variety of bicontinuous cubic phases by rationally altering the relative content of inorganic and organic components in the hybrids.[28]

In contrast, the realization of the inverse bicontinuous structures where the inorganic components occupy the channels (that is, the minority volume fraction) has been much more challenging. Most approaches have been based either on thin films[17] that cannot be easily extended to the bulk or negative replication of the parent mesophase which becomes the sacrificial mold.[14–16] Negative replication using impregnation and other techniques, apart from being tedious, gives rise to large-scale imperfections and defects in the resulting strut networks. Herein we present a simple and direct approach to bicontinuous 3D connected robust network struts starting from a cubic bicontinuous bulk hybrid material for which structural data is consistent with the plumber's nightmare morphology that is subsequently heat-treated at high temperatures without loss of the structural symmetry.

[*] A. Jain, S. Mahajan, C. B. W. Garcia, U. Wiesner
Department of Materials Science and Engineering, Bard Hall
Cornell University
Ithaca, NY 14853 (USA)
Fax: (+1) 607-255-2365
E-mail: ubw1@cornell.edu

G. E. S. Toombes, S. M. Gruner
Department of Physics, Clark Hall
Cornell University, Ithaca, NY 14853 (USA)

L. M. Hall
Rose-Hulman Institute of Technology
Terre Haute, IN 47803 (USA)

W. Probst
Consulting & Education in Microscopy
Digital Imaging and Analysis, Essingen (Germany)

Monodisperse poly(isoprene-b-ethylene oxide) (PI-b-PEO), synthesized anionically (polydispersity < 1.1) with a total molecular weight of $19\,900\ \mathrm{g\,mol^{-1}}$ and PEO volume fraction, f_{PEO}, of 0.15, was used as the structure-directing agent. The pure diblock copolymer exhibits a BCC morphology in the melt consisting of PEO spheres in a PI matrix. Sol–gel synthesis was carried out by mixing the polymer with ormocer precursor, (3-glycidyloxypropyl) trimethoxysilane (GLYMO) and aluminum *sec*-butoxide in a molar ratio of 80:20 following a procedure described elsewhere.[7] The procedure used herein differs from that reported in that the evaporation of the solvents before the final condensation step was carried out in a rotating cylindrical Büchi evaporator under controlled vacuum. Assuming negligible phase mixing between the PI (density $0.91\ \mathrm{g\,cm^{-3}}$) and the inorganic/PEO microphases (density $1.4\ \mathrm{g\,cm^{-3}}$),[29] the volume fraction of the PEO/inorganic phase in the as-made material was calculated to be 0.37. This is very close to the volume fraction of the PI channels (0.36 and 0.37) in the plumber's nightmare morphology.[13,28] The as-made hybrid sample was then calcined by heating to $600\,^\circ\mathrm{C}$ in several steps which pyrolyzed the organic components and left the bicontinuous skeletal networks of silica.

SAXS experiments were performed on both the as-made and calcined samples to determine the underlying symmetry of the nanostructured materials. Azimuthally integrated scattering profiles of X-ray scattering intensity, I, versus the magnitude of the scattering vector, $q = (4\pi/\lambda)\sin\theta$, where λ is the X-ray wavelength and 2θ is the scattering angle, for the as-made and the calcined samples are shown in Figure 1. As is typically the case for copolymer diffraction, the powder diffraction patterns yield too few orders to unambiguously assign a lattice symmetry. However, even a small number of rings allows the exclusion of most symmetries. The most intense and unambiguous reflections in Figure 1a have the distance ratios of $\sqrt{2}$, $\sqrt{6}$, $\sqrt{8}$, and $\sqrt{14}$. These ratios are consistent with the $Im\bar{3}m$ space group and inconsistent with the $Ia\bar{3}d$ gyroid-like symmetry. The unit cell size (73 nm) and relative peak intensities are quite similar to the more rigorously characterized regular structure that was assigned to the plumber's nightmare morphology.[28] The scattering profile of the calcined material in Figure 1b differs considerably from the parent material. The most intense peaks have the distance ratios of $\sqrt{2}$, $\sqrt{4}$, $\sqrt{6}$, $\sqrt{8}$, and $\sqrt{12}$ with some scattering features also evident at $\sqrt{14}$. This is again consistent with the $Im\bar{3}m$ space group with a unit cell size of 47 nm. It corresponds to a shrinkage of the unit cell size by approximately 36 % relative to the uncalcined material and is similar to calcination results on such block copolymer derived ormocer materials.[28] The considerable change in the relative peak intensities is indicative of a significant variation in the structure factor of the calcined mesophase from the parent material. The plasticizing effect of the polymer chains on the ceramic in these materials was recently demonstrated by solid-state NMR spectroscopy.[30] The changes in the scattering amplitude may reflect the ability of the ceramic to readjust and perfect the structure during calcination from the parent "flexible ceramic" nanocomposites.

In a number of calcined samples, individual crystallites were large enough that Bragg Peaks were observed (Fig-
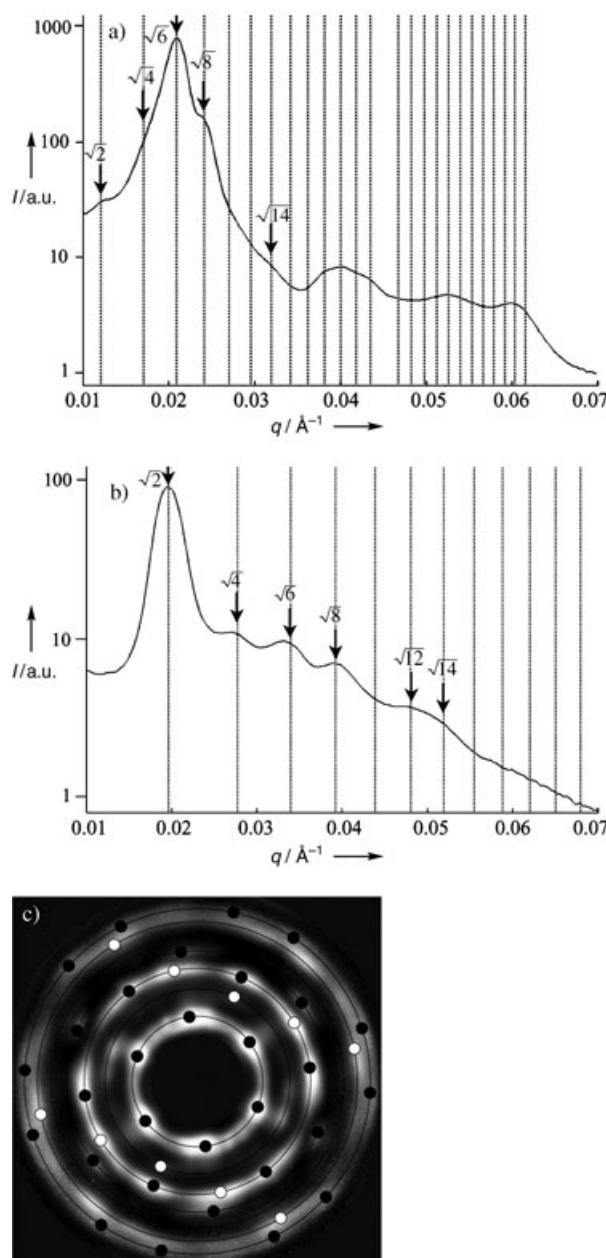

Figure 1. Azimuthally integrated scattering profile (X-ray intensity I versus scattering wave vector q) measured for the a) as-made and b) calcined samples. The vertical dotted lines correspond to the expected peaks for $Im\bar{3}m$ crystallographic space group. c) 2D SAXS pattern of the calcined sample. The markers correspond to the indexed peak positions for the calcined sample (see text for explanation). The radii of the circles q are given by $q = \sqrt{h^2 + k^2 + l^2}$, where h, k, and l are integers allowed by the $Im\bar{3}m$ symmetry group.

ure 1c). The pronounced sixfold symmetry of the diffraction image reflects the threefold symmetry ({111} zone direction) of a cubic crystal. The black markers in Figure 1c locate the six $\sqrt{2}$ [110], six $\sqrt{8}$ [211], six $\sqrt{8}$ [220], and twelve $\sqrt{14}$ [321] peaks permitted in the $Im\bar{3}m$ space group. While there is no unique indexing for a diffraction pattern generated by multiple crystallites, most of the diffraction spots in Figure 1c were generated by a single crystallite. The white markers (zone direction [110]) illustrate how a second crystallite might

account for many of the remaining diffraction spots. Clearly, however, more than two crystallites contributed to the diffraction pattern. In other diffraction images, the fourfold symmetry axis of the $Im\bar{3}m$ space group has been observed (data not shown). These symmetries give us considerable confidence that the unit cell is cubic. The $\sqrt{2}$, $\sqrt{4}$, and $\sqrt{12}$ peaks eliminate the $Ia\bar{3}d$ (gyroid) space group while the space group $Pn\bar{3}m$ (double diamond) seems quite unreasonable given the systematic absence of $\sqrt{3}$, $\sqrt{9}$, and $\sqrt{11}$ peaks. The peaks and symmetries observed in the diffraction data are thus fully consistent with the $Im\bar{3}m$ (plumber's nightmare) space group.

The shrinkage of the unit cell volume and the association of the inorganic material with the minority fraction suggest that the calcined samples preserve the strut structure of the sample, which is the reverse of what has been observed when the PEO + inorganic component is the majority fraction. It is remarkable that calcination leaves behind the two discrete interwoven networks intact without collapsing on each other. We speculate that they are held in place by the grain boundaries. The absence of collapse of the network structure is corroborated by the high surface area indicated by nitrogen sorption/desorption measurements. Indeed, the calcined sample exhibits a nitrogen-sorption isotherm of type IV according to BDDT classification, with a specific surface area of 295 $m^2 g^{-1}$ according to the Brunauer–Emmett–Teller (BET) method (data not shown).[31]

To elucidate further the structure in real space, we have performed TEM on bulk, calcined, and solvent-dispersed samples. Figure 2 a and b show two dark-field projections of the bulk as-made composite. The continuity of the silica networks (white struts) in the underlying structure is clearly observed in both images. The TEM image and its autocorrelation (inset) in Figure 2 b indicate that the struts form a lattice of similar size to that determined by SAXS (some lattice distortion is expected from the sample and TEM
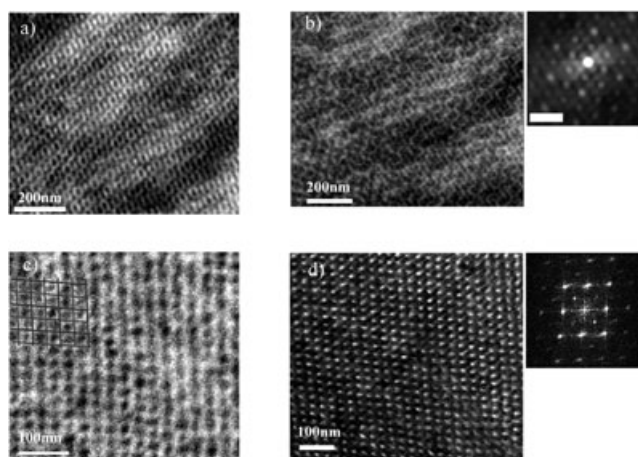

Figure 2. a) Dark-field TEM image of the as-made sample showing the continuous network structure. b) Dark-field image of the as-made sample showing network-struts. The inset shows the autocorrelation of the image; scale bar 100 nm. c) Dark-field image of the calcined sample. The black and the gray lines indicate the individual networks contained in the bicontinuous lattice. d) Bright-field image of the calcined sample. The inset shows the computed Fourier transform image.

specimen preparation method[28]). Figure 2 c shows a dark-field image of the calcined sample and indicates the individual networks that compose the mesophase. A bright-field image of the calcined sample is shown in Figure 2 d. Despite minor distortion of the sample, the underlying lattice is clearly discernable. The peaks in the corresponding Fourier transform image (Figure 2 d inset) give a consistent fit to a lattice of the $Im\bar{3}m$ space group with a side of 51 nm. This is within close tolerance of the value determined from SAXS.

The presence of the organic matrix around the silica channels can be used for dispersing the sample in an organic solvent, such as toluene. By sonicating a piece of the as-made sample in toluene, the network structure could be ripped apart and a colloidal solution was obtained. Such dispersion provides direct visualization of the network struts when viewed under TEM. Figure 3 a–c show bright-field images of
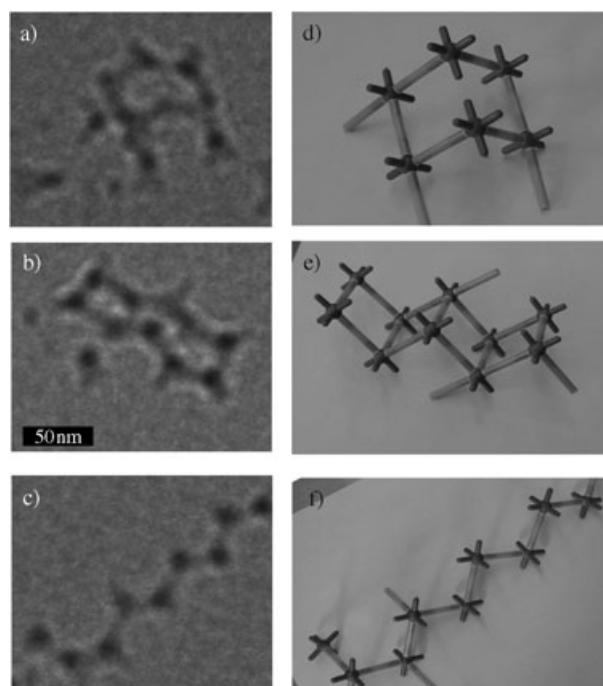

Figure 3. Bright-field TEMs of the broken network structure (a–c) dispersed in a toluene solution, and the corresponding projections from a bead–stick model (d–f). The scale bar in (b) is the same for all TEMs. The distance measured between the nodes are in accord with the expected value from SAXS and TEM measurements.

different broken network struts. The struts appear as light-gray lines connected together at junctions that resolve as dark spots in the TEM image. These images further confirm the skeletal character of the structure. As shown in Figure 3 d–f, struts and junctions from a bead-and-stick model of the $Im\bar{3}m$ lattice can be assembled into matching projections.

In summary, we have demonstrated a simple and direct approach to thick samples of robust skeletal silica-based bicontinuous nanostructures. By using a combination of SAXS and TEM, the structure of the mesophase was found to be most consistent with the $Im\bar{3}m$ cubic space group associated with the plumber's nightmare morphology (Figure 4 b) based on the "P" minimal surface (Figure 4 a). The
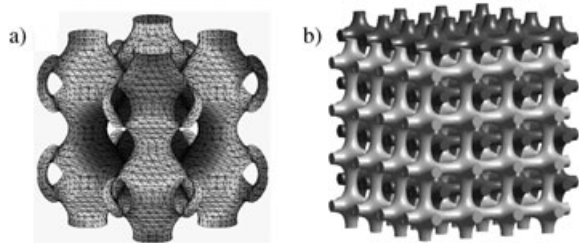
Figure 4. a) The "P" minimal surface. b) A skeletal structure of the plumber's nightmare with the networks occupying 37% of the volume.

existence of the bicontinuous structure in the reverse phase points towards the versatility and the generality of the phase space attainable by ormocer-derived organic–inorganic hybrid materials. Structural integrity was preserved in the thick samples after calcination although the inorganic constituent formed the minority phase. Nitrogen-sorption isotherms demonstrated a large surface area associated with these networks. These periodic and interconnected networks also have potential as photonic band-gap materials.[32]

Experimental Section

SAXS data were collected on a Rigaku RU300 copper rotating-anode ($\lambda = 1.54$ Å) operated at 40 kV and 50 mA. X-rays were monochromatized with a Ni filter and focused using orthogonal Franks mirrors. SAXS patterns were collected with a homebuilt $1\,K \times 1\,K$ pixel CCD detector.[33]

For TEM of the bulk samples, 50–100 nm sections were cut using a Leica Ultracut UCT microtome at 210 K (as-made composite) and 300 K (skeletal networks) and transferred to copper grids. TEM was performed on a Leo 922 Ω (tungsten filament) microscope at 200 kV using an objective aperture angle of 3.6 mrad. Images were taken in both the elastic filtering as well as the inelastic energy-loss imaging mode using a slow-scan CCD camera (lateral resolution $2\,K \times 2\,K$ pixels). A value of ΔE of 120–145 eV around the Si K edge was chosen for the images taken in the energy-loss mode. To image broken pieces of the network structure, samples were dispersed in toluene by stirring and sonication. The resulting colloidal suspension was transferred on carbon-coated grids. For ease in imaging, the grids were subjected to UV-ozonolysis/calcination to remove the organics before imaging under a JEOL 1200EX microscope operating at 120 kV in the bright-field mode.

Nitrogen adsorption and desorption isotherms were measured on a Micromeritics ASAP 2020 at 77 K after outgassing at 100 mPa for 15 h at 523 K.

[1] H. Eckert, M. D. Ward, *Chem. Mater.* **2001**, *13*, 3059.
[2] C. T. Kresge, M. E. Leonowicz, W. J. Roth, J. C. Vartuli, J. S. Beck, *Nature* **1992**, *359*, 710.
[3] A. Monnier, F. Schüth, Q. Huo, D. Kumar, D. Margolese, R. S. Maxwell, G. D. Stucky, M. Krishnamurthy, P. Petroff, A. Firouzi, M. Janicke, B. F. Chmelka, *Science* **1993**, *261*, 1299.
[4] S. A. Bagshaw, E. Prouzet, T. J. Pinnavaia, *Science* **1995**, *269*, 1242.
[5] D. Zhao, J. Feng, Q. Huo, N. Melosh, G. H. Fredrickson, B. F. Chmelka, G. D. Stucky, *Science* **1998**, *279*, 548.
[6] L. Bronstein, E. Krämer, B. Berton, C. Burger, S. Förster, M. Antonietti, *Chem. Mater.* **1999**, *11*, 1402.
[7] M. Templin, A. Franck, A. Du Chesne, H. Leist, Y. Zhang, R. Ulrich, V Schädler, U. Wiesner, *Science* **1997**, *278*, 1795.
[8] Y.-T. Chan, H.-P. Lin, C.-Y. Mou, S.-T. Liu, *Chem. Commun.* **2002**, *23*, 2878.
[9] X. Liu, B. Tian, C. Yu, F. Gao, S. Xie, B. Tu, R. Che, L. Peng, D. Zhao, *Angew. Chem.* **2002**, *114*, 4032; *Angew. Chem. Int. Ed.* **2002**, *41*, 3876.
[10] K. Flodstroem, V. Alfredsson, N. Kaellrot, *J. Am. Chem. Soc.* **2003**, *125*, 4402.
[11] C. Yu, Y. Yu, D. Zhao, *Chem. Commun.* **2000**, *7*, 575.
[12] D. Zhao, Q. Huo, J. Feng, B. F. Chmelka, G. D. Stucky, *J. Am. Chem. Soc.* **1998**, *120*, 6024.
[13] A. C. Finnefrock, R. Ulrich, A. Du Chesne, C. C. Honeker, K. Schumacher, K. K. Unger, S. M. Gruner, U. Wiesner, *Angew. Chem.* **2001**, *113*, 1247; *Angew. Chem. Int. Ed.* **2001**, *40*, 1208.
[14] B. Tian, X. Liu, L. A. Solovyov, Z. Liu, H. Yang, Z. Zhang, S. Xie, F. Zhang, B. Tu, C. Yu, O. Terasaki, D. Zhao, *J. Am. Chem. Soc.* **2004**, *126*, 865.
[15] S. Che, A. E. Garcia-Bennett, X. Liu, R. P. Hodgkins, P. A. Wright, D. Zhao, O. Terasaki, T. Tatsumi, *Angew. Chem.* **2003**, *115*, 4060; *Angew. Chem. Int. Ed.* **2003**, *42*, 3930.
[16] S. C. Laha, R. Ryoo, *Chem. Commun.* **2003**, *17*, 2138. See also F. Schüth, *Angew. Chem.* **2003**, *115*, 3730; *Angew. Chem. Int. Ed.* **2003**, *31*, 3604
[17] V. Z. H. Chan, J. Hoffman, V. Y. Lee, H. Iatrou, A. Avgeropoulos, N. Hadjichristidis, R. D. Miller, E. L. Thomas, *Science* **1999**, *286*, 1716.
[18] D. A. Huse, L. Stanislas, *J. Phys.* **1988**, *49*, 605.
[19] J. Seddon, R. Templer, *New Sci.* **1991**, *45*, 1769.
[20] C. B. W. Garcia, Y. Zhang, F. DiSalvo, U. Wiesner, *Angew. Chem.* **2003**, *115*, 1564; *Angew. Chem. Int. Ed.* **2003**, *42*, 1526.
[21] C. B. W. Garcia, C. Lovell, C. Curry, M. Faught, Y. Zhang, U. Wiesner, *J. Polym. Sci. Part B* **2003**, *41*, 3346.
[22] E. L. Thomas, D. M. Anderson, C. S. Henkee, D. Hoffman, *Nature* **1988**, *334*, 598.
[23] A good source for mathematical description and visualization of bicontinuous mesophases is available at http://www.msri.org/publications/sgp/SGP/
[24] P. Ström, D. M. Anderson, *Langmuir* **1992**, *8*, 691.
[25] I. W. Hamley, *The Physics of Block Copolymers*, Oxford University Press, Oxford, **1998**.
[26] D. A. Hajduk, P. E. Harper, S. M. Gruner, C. C. Honeker, G. Kim, E. L. Thomas, L. J. Fetters, *Macromolecules* **1994**, *27*, 4063.
[27] C. Garcia, R. Ulrich, M. Kamperman, A. Jain, U. Wiesner, unpublished results.
[28] A. C. Finnefrock, R. Ulrich, G. E. S. Toombes, S. M. Gruner, U. Wiesner, *J. Am. Chem. Soc.* **2003**, *125*, 13084.
[29] R. Ulrich, A. Du Chesne, M. Templin, U. Wiesner, *Adv. Mater.* **1999**, *11*, 141.
[30] S. M. De Paul, J. W. Zwanziger, R. Ulrich, U. Wiesner, H. W. Spiess, *J. Am. Chem. Soc.* **1999**, *121*, 5727.
[31] S. Brunauer, L. S. Deming, W. S. Deming, E. Teller, *J. Am. Chem. Soc.* **1940**, *62*, 1723.
[32] M. Maldovan, A. M. Urbas, N. Yufa, W. C. Carter, E. L. Thomas, *Phys. Rev. B* **2002**, *65*, 165123.
[33] M. W. Tate, S. M. Gruner, E. F. Eikenberry, *Rev. Sci. Instrum.* **1997**, *68*, 47.